Research article 2019 Ridgecrest earthquake sequence

Catalog dependence of early aftershock decay in the 2019 Ridgecrest sequence

Abstract

The time distribution of reported earthquakes depends on catalog construction. We test whether that dependence changes the inferred decay of reported aftershocks following the Ridgecrest mainshock. We compared the USGS Comprehensive Earthquake Catalog (ComCat) and the Shelly template-matched and relocated release over nine days following the 6 July 2019 M_w 7.1 Ridgecrest mainshock. The relocated data contained 25,268 events of any reported magnitude in the spatial window, versus 14,267 in ComCat. During the first 15 minutes the ordering reversed, with 27 versus 66 records. At a nominal magnitude threshold of 1.5, power laws fitted to hours 1–72 gave effective decay exponents of 0.481 and 0.550, respectively. The relocated exponent was lower at all 25 combinations of five thresholds and five start times, with differences of approximately -0.40 to -0.01. Extrapolation to hours 72–216 overcounted recorded events by 71% in the relocated catalog and 33% in ComCat. The catalogs share events and differ in processing and magnitude reporting, so the contrasts do not identify detection probabilities or the physical decay exponent.

Primary comparison	ComCat	Shelly
Effective exponent, hours 1–72, $M \geq 1.5$	0.550	0.481
Recorded events, hours 1–72, $M \geq 1.5$	4,869	5,112
Observed / extrapolated events, hours 72–216	0.753	0.586

1. Introduction

During the first hours after a large earthquake, a rate curve reflects both physical clustering and the ability of a seismic network and its processing workflow to separate nearby signals. These processes are difficult to distinguish for Ridgecrest, where an M_w 6.4 rupture on 4 July 2019 was followed about 34 hours later by an M_w 7.1 earthquake in a system of intersecting faults. Ross et al. (2019) mapped the ruptures and showed short-term catalog incompleteness in their magnitude–time overview. Van der Elst and Page (2023) used the same sequence to demonstrate a rate estimator designed to reduce sensitivity to rapid changes in catalog completeness. Shelly's (2020a, 2020b) relocation study emphasized fault geometry and released event times, locations and magnitudes suitable for comparing two public representations of the same interval.

An enhanced catalog that preferentially adds early small events might have a steeper apparent decay than a routine catalog at a fixed magnitude threshold. A gain in total records alone gives no evidence about when the extra records occur. Recovery can vary with time, and template construction, relative relocation and magnitude assignment affect which records pass a given cut. We compare the cataloged time profiles under common geographic bounds, a common mainshock clock and identical nominal magnitude thresholds. We examine the direction and size of the change in decay exponent across a specified grid, supported by raw counts and a held-time check on the single-slope model.

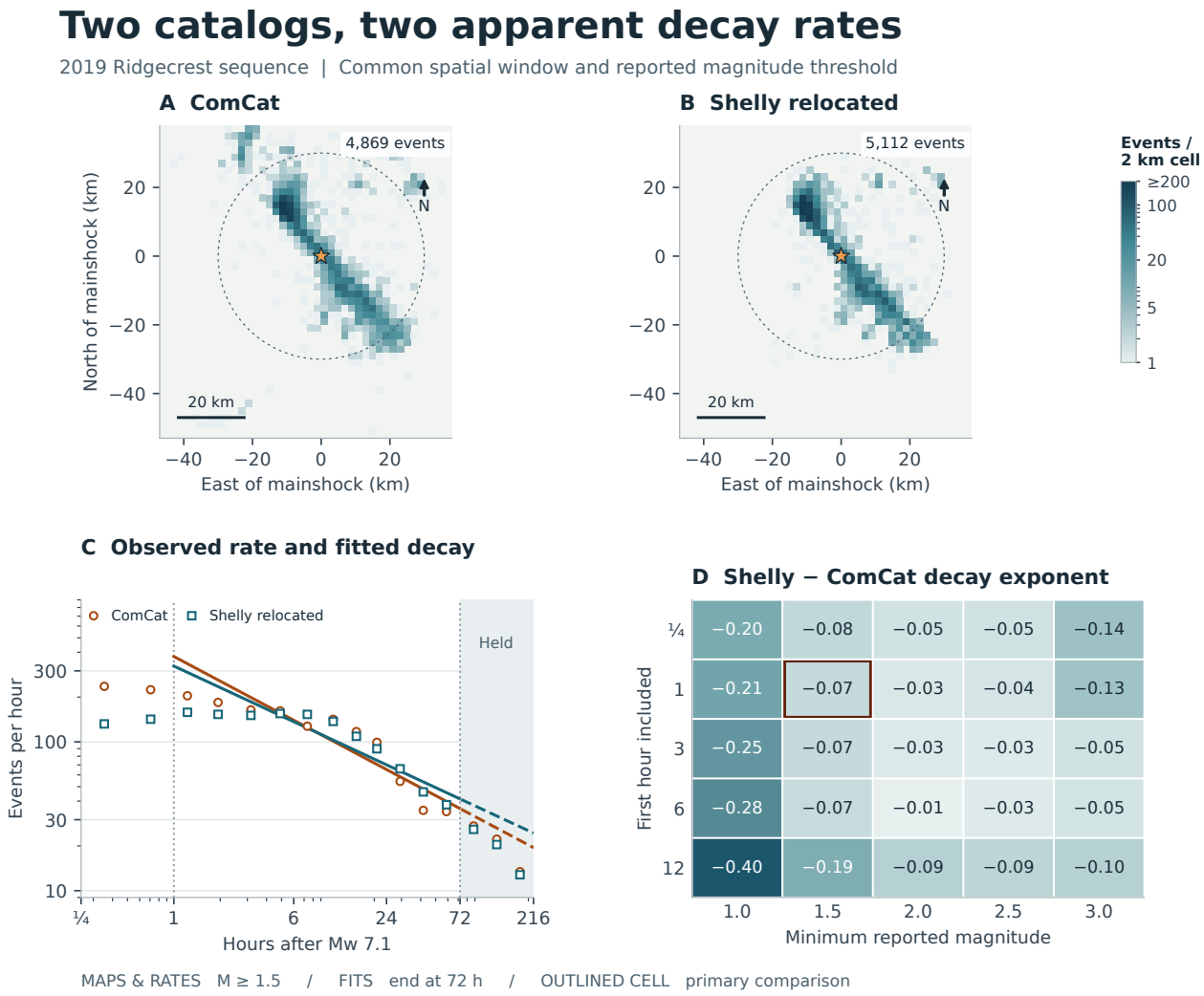


Figure 1. Spatial and temporal comparison at shared selection settings. (A–B) Counts in 2 km by 2 km cells in an azimuthal-equidistant projection. Grid shading shows recorded events per cell. Both panels show the mainshock (star) and the central 30 km sensitivity region (dotted circle). Maps and fits use reported $M \geq 1.5$ and hours 1–72. (C) Duration-normalized counts at geometric bin midpoints. Dashed lines extrapolate fitted rates through the shaded held interval. (D) Differences in exponents across thresholds and fit starts. Negative entries indicate a shallower relocated profile. The outlined cell denotes the primary comparison.

2. Data and methods

Time and spatial selection. The preferred ComCat origin for event ci38457511 defines $t = 0$ at 03:19:53.040 UTC on 6 July 2019. The common selection is $0 < t < 216$ h, 35.3–36.1° N and 118.1–117.2° W. We query the FDSN interface for earthquake-type events and select the preferred location and magnitude fields. The Shelly data use waveform templates from 13,525 routinely cataloged events and list 34,091 hypocentroids before filtering. We drop the ComCat mainshock by identifier and exclude any $M \geq 6$ record in the first minute to guard against a shifted mainshock origin. The spatial check restricts the primary selection to a 30 km radius using a spherical Earth of radius 6371.0088 km.

Magnitudes and models. The selected ComCat entries include 13,968 ML, 205 MLR, 80 MW and 14 MH magnitudes as labeled by the FDSN service. We excluded the mainshock before counting these entries. Shelly retained the preferred Southern California Seismic Network magnitudes for events already in its parent catalog and calibrated magnitudes of new detections to a local scale using an amplitude relation stated in the release. We apply identical *reported* magnitude cuts and preserve the catalogs' numerical precision. A nominal cutoff does not guarantee completeness or magnitude equivalence.

For cataloged times $t_i \in [a, 72)$ h we fit the descriptive intensity $\lambda(t) = K(t + c)^{-p}$, a modified Omori form (Utsu et al., 1995). We fix $c = 0$ so the profile over positive time has a single shape parameter. For a curvature check we fix $c = 1$ h and re-estimate p. With $I(u, v; p, c) = \int_u^v (t+c)^{-p}\, dt$ and n training events, the profile negative log-likelihood is

$$\mathcal{L}(p) = p \sum_i \log(t_i + c) + n \log I(a, 72; p, c)$$

up to terms independent of p. The amplitude estimate is $\widehat{K} = n/I(a, 72; \widehat{p}, c)$, and the held-period expectation is $\widehat{K} I(72, 216; \widehat{p}, c)$. For $p = 1$, I is the log ratio of the shifted bounds. The equation supplies a descriptive projection of an observed profile. Event clustering and catalog dependence within one sequence motivate reporting specification sensitivity and temporal misfit in place of event-level standard errors or cross-sequence significance tests.

The primary reported magnitude cutoff is 1.5 and the starting time is 1 h. We cross thresholds $1, 1.5, 2, 2.5, 3$ with starts $0.25, 1, 3, 6, 12$ h. Each contrast is $p_{\text{Shelly}} - p_{\text{ComCat}}$ and the fit ends at hour 72 throughout. A separate diagnostic compares counts and the within-catalog share of entries with $M < 1.5$ in fixed windows.

3. Results

3.1 Reversal of the count ordering

In the first hour ComCat contained 237 events of any magnitude and the relocated catalog 131. In the first quarter-hour all 66 ComCat and all 27 relocated entries were at or above 3.0, causing all threshold-specific ratios to coincide. In hours 24–72 the relocated-to-ComCat count ratio was 1.76 at $M \geq 1$ and 0.94 at $M \geq 3$. The share of small entries changed sharply over the interval (Fig. 2). The sign of the count difference changes at fixed cuts without a change in geographical selection.

3.2 A consistent sign with a variable size

Under the main specification, p was 0.550 in ComCat and 0.481 in the relocated catalog ($\Delta p = -0.070$). Both fitted curves miss early and late behavior, and the fitted ranking reverses within the window (Fig. 1C). Restricting the window to within 30 km of the mainshock gave 0.570 and 0.494, respectively. Fixing c at 1 h increased both exponents to 0.627 and 0.547, respectively. The fitted exponent was lower in the relocated catalog at all 25 threshold and start combinations. The largest difference occurred for a 12 h start and threshold 1.0, and the smallest occurred for a 6 h start and threshold 2.0. At a common 6 h start the gap was about 0.28 at 1.0 and about 0.01 at 2.0 (Fig. 1D).

3.3 Temporal check on the fitted profiles

The hour 72–216 catalog totals were 2,744 and 2,586, and the preceding fits implied about 3,644 and 4,411. Actual counts were 75.3% and 58.6% of those extrapolations, respectively. The $c = 1$ h sensitivity moved the ratio closer to one to 83.1% for ComCat and 63.8% for the relocated catalog. This mismatch is visible in the late-bin rates and shows why proximity of two fitted exponents alone is insufficient to assess how well either model represents the time profile.

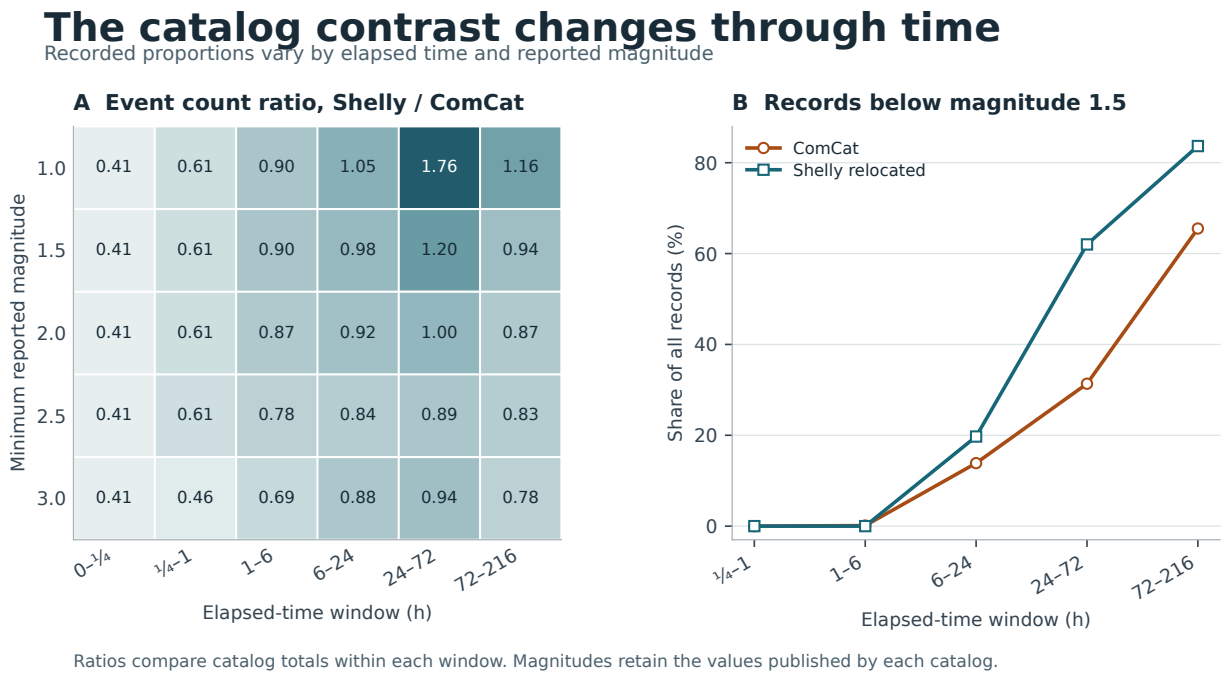


Figure 2. Catalog disagreement by elapsed time and reported magnitude. (A) Each cell divides the number of relocated records by the number of ComCat records at or above the indicated cut. (B) Percentage of records below 1.5 among all reported magnitudes. Both catalogs have zero such entries in the first 15 minutes, which are omitted from (B).

Table 1. Counts by elapsed-time window at reported $M \geq 1.5$.

Hours	ComCat	Shelly	Shelly / ComCat
0–0.25	66	27	0.409
0.25–1	171	104	0.608
1–6	855	768	0.898
6–24	2,131	2,092	0.982
24–72	1,883	2,252	1.196
72–216	2,744	2,586	0.942

4. Discussion

The catalog with more records overall assigns less weight to the immediate post-mainshock period and gives a shallower apparent decay at every examined setting. The count diagnostics show the counterweight to its overall enrichment. In the first quarter hour, when phases are difficult to separate against the mainshock coda, ComCat includes over twice as many events as the relocated file. Differences persist above the lowest cut. At 24–72 h the relocated release exceeds ComCat at 1.0 and 1.5, nearly ties at 2.0 and falls below it at higher cuts. The ratio varies through time at a fixed threshold and varies by threshold within the same window. These two dependencies explain why an event-count comparison over the entire period gives little guidance about the rank of fitted exponents.

Van der Elst and Page (2023) independently document short-term incompleteness in this sequence, and Ross et al. (2019) document the rupture geometry and off-fault activity. The sources motivate distinct issues here. A large-event coda can suppress ordinary detection, and the template-matching and relocation product has its own selection. Regional counts can also combine seismicity from multiple spatial clusters or ruptures. The 30 km analysis indicates that events in the outer box are unnecessary for the main sign. Neither the spatial check nor the monotonic models trace which prior rupture triggered particular events. We use aftershocks as an operational term for earthquakes in the space-time window. Background seismicity and secondary triggering may contribute.

Limitations

The catalogs use related waveforms and share an unknown number of entries within each threshold and time window. A raw count ratio compares two totals with unknown overlap. In hours 6–24 at reported $M \geq 1.5$, the ratio is $2{,}092/2{,}131 = 0.982$. The denominator is the ComCat count, and the numerator counts every eligible relocated entry regardless of whether it also appears in ComCat. Estimating completeness requires an estimate of the number of eligible earthquakes that actually occurred. Distinct event association, preferred-magnitude changes, relative relocation across boundaries and calibration of new detections can influence those totals. Neither release is a reference set for measuring absolute recovery in the other. Establishing the contribution of each mechanism would require event associations and independent checks such as magnitude cross-calibration and a waveform recovery study. The held-time discrepancy also leaves open contributions from nonstationary detection or real changes in the mix of aftershocks. The fitted exponents summarize the archived records in this sequence.

Conclusions

The same region and nominal cutoff yielded distinct profiles for the first three days of the Ridgecrest sequence. A higher total count can coexist with fewer records immediately after the mainshock, shallower fitted decay and a greater overcount when a single power law is projected forward. Analysts comparing early aftershock decay can reveal this dependence by reporting elapsed-time counts, catalog and magnitude provenance, and sensitivity to the fit start alongside the exponent.

Data and code availability

The USGS catalog snapshot was acquired on 14 November 2026 through the FDSN event service. ComCat updates preferred values, so the code records the query and original SHA-256. Shelly's `DataS1_noXYZ.txt` is released by USGS under CC0 and archived at 10.5066/P9JN6H0N. The source bundle contains executable analysis and figure code, aggregate results and links and hashes for both inputs.

References

Ross, Z. E., et al. (2019). Hierarchical interlocked orthogonal faulting in the 2019 Ridgecrest earthquake sequence. *Science*, 366(6463), 346–351. 10.1126/science.aaz0109.

Shelly, D. R. (2020a). A high-resolution seismic catalog for the initial 2019 Ridgecrest earthquake sequence. U.S. Geological Survey data release. 10.5066/P9JN6H0N.

Shelly, D. R. (2020b). A high-resolution seismic catalog for the initial 2019 Ridgecrest earthquake sequence: Foreshocks, aftershocks, and faulting complexity. *Seismological Research Letters*, 91(4), 1971–1978. 10.1785/0220190309.

Utsu, T., Ogata, Y., & Matsu'ura, R. S. (1995). The centenary of the Omori formula for a decay law of aftershock activity. *Journal of Physics of the Earth*, 43(1), 1–33. 10.4294/jpe1952.43.1.

van der Elst, N. J., & Page, M. T. (2023). a-positive: A robust estimator of the earthquake rate in incomplete or saturated catalogs. *Journal of Geophysical Research: Solid Earth*, 128(10), e2023JB027089. 10.1029/2023JB027089.